Amino Acids (2012) 43:603–615
DOI 10.1007/s00726-011-1108-7

ORIGINAL ARTICLE

In silico investigation of molecular mechanism of laminopathy caused by a point mutation (R482W) in lamin A/C protein

Vidya Rajendran · Rituraj Purohit · Rao Sethumadhavan

Received: 16 June 2011 / Accepted: 24 September 2011 / Published online: 12 October 2011

Abstract Lamin A/C proteins are the major components of a thin proteinaceous filamentous meshwork, the lamina, that underlies the inner nuclear membrane. A few specific mutations in the lamin A/C gene cause a disease with remarkably different clinical features: FPLD, or familial partial lipodystrophy (Dunnigan-type), which mainly affects adipose tissue. Lamin A/C mutant R482W is the key variant that causes FPLD. Biomolecular interaction and molecular dynamics (MD) simulation analysis were performed to understand dynamic behavior of native and mutant structures at atomic level. Mutant lamin A/C (R482W) showed more interaction with its biological partners due to its expansion of interaction surface and flexible nature of binding residues than native lamin A/C. MD simulation clearly indicates that the flexibility of interacting residues of mutant are mainly due to less involvement in formation of inter and intramolecular hydrogen bonds. Our analysis of native and Mutant lamin A/C clearly shows that the structural and functional consequences of the mutation R482W causes FPLD. Because of the pivotal role of lamin A/C in maintaining dynamics of nuclear function, these differences likely contribute to or represent novel mechanisms in laminopathy development.

Keywords Docking simulation · Laminopathy · RMSD · SASA

V. Rajendran · R. Purohit · R. Sethumadhavan (✉)
Bioinformatics Division, School of Bio Sciences and Technology, Vellore Institute of Technology University, Vellore 632014, Tamil Nadu, India
e-mail: rsethumadhavan@vit.ac.in

Introduction

The nuclear envelope of eukaryotes is composed of membranes, nuclear pores and a nuclear lamina. The nuclear lamina is a dense filamentous network underlying the inner nuclear membrane and is mainly composed of intermediate filament (IF)-type proteins, the lamins (Newport et al. 1990). Lamins feature the typical structure of IF that constitutes an N-terminal "head domain", a central alphahelical "coiled coil" rod domain and a carboxy-terminal "tail domain" (Strelkov et al. 2003). Numerous functions are performed by lamins, including maintaining stability of the nuclear structure, organization of chromatin, regulation of cell cycle (Burke and Stewart 2002), apoptosis and various biochemical and metabolic processes (Cohen et al. 2001); they are also implicated in the regulation of gene expression, DNA replication and mRNA transcription (Maraldi et al. 2007).

Specific missense mutations in the lamin A/C gene have been shown to cause Dunnigan-type familial partial lipodystrophy type 2 (FPLD2: OMIM No. 151660) (Cao and Hegele 2000; Shackleton et al. 2000; Speckman et al. 2000). It is a rare autosomal dominant disease, which is part of a heterogeneous group of disorders characterized by complete or partial absence of adipose tissue (Kobberling and Dunnigan 1986; Burn and Baraitser 1986). Patients with FPLD are born with normal fat distribution, but with the onset of puberty, they start losing subcutaneous fat from their extremities, trunk and gluteal region (Kobberling and Dunnigan 1986; Garg et al. 1999). Also, excess fat may become deposited in the face, neck, back and labia majora and lead to disfigurement (Kobberling and Dunnigan 1986; Burn and Baraitser 1986; Garg et al. 1999; Jacob and Garg 2006). Findings indicated that transcriptional activity of several genes involved in adipogenesis is altered in the

affected tissues of patients with FPLD2 (Araújo-Vilar et al. 2009) and patients with decreased subcutaneous adipose tissue in the limbs and trunk were reported (Lado-Abeal et al. 2010). Neuromuscular and cardiac dystrophies, lipodystrophies, and premature ageing syndromes (Vantyghem et al. 2004) and loss of subcutaneous fat and muscular hypertrophy, especially of the lower extremities, started as early as in childhood, acanthosis and severe hypertriglyceridemia developed later in life, followed by diabetes are indicated by FPLD patients (Schmidt et al. 2001). Prevalence of goiter tended to be higher in LMNA-mutated than in non-mutated subjects (Vantyghem et al. 2007). FPLD results from heterozygous missense mutations in the lamin A/C gene, mapped to chromosome 1q21–q23 (Cao and Hegele 2000; Speckman et al. 2000; Shackleton et al. 2000; Vigouroux et al. 2000; Hegele 2001). By alternative splicing, *LMNA* gives rise to different types of A lamins; the main isoforms are lamin A and lamin C, which only differ in their C-terminal amino acids. These ubiquitous intermediate filamentous proteins homo- and hetero-polymerize with B-type lamins to form the nuclear lamina, a meshwork underlying the inner nuclear membrane, where they interact with integral proteins such as emerin (Stuurman et al. 1998; Sakaki et al. 2001; Frock et al. 2006) and sterol regulatory element-binding protein 1 (SREBP1) (Stuurman et al. 1998; Lloyd et al. 2002). The FPLD-linked lamin A/C mutations are mainly located within a highly conserved region (in exon 8) of the gene, coding for the proximal c-terminal domain of A-type lamins. Approximately 90% of LMNA mutations that cause FPLD are localized to exon 8 and occur at amino acid 482 (Prokocimer et al. 2009). Out of the three mutations (R482W/Q/L) that cause FPLD, R482W is the one that is most frequently found (Cao and Hegele 2000; Hegele et al. 2000a, b).

The structure of the globular tail of lamin A/C reveals a compact, well-defined domain composed entirely of β strands (Dhe-Paganon et al. 2002). Two large β sheets form a β sandwich. One sheet has five β strands and the other has four. A second, smaller β sheet lies perpendicular and adjacent to the plane of the β sandwich. Short loops connect most of the β strands, leading to the compact appearance of the domain and it is depicted in Fig. 1.

Previous studies suggest SREBP1 and emerin as a novel interacting partner of lamin A/C (Sullivan et al. 1999; Lloyd et al. 2002; Nikolova et al. 2004). SREBP1 is a dual specificity transcription factor of the basic helix–loop–helix leucine zipper family that has independently been shown to be involved in both the regulation of cholesterol biosynthesis (Yokoyama et al. 1993) and in adipogenesis, including the expression of genes involved in fatty acid metabolism (Yokoyama et al. 1993; Kim and Spiegelman 1996). The helix–loop–helix motif of SREBP1 between residues 337 and 374 interacts with c-terminal domain of lamin A/C (Sullivan et al. 1999; Lloyd et al. 2002; Nikolova et al. 2004). FPLD mutations had no effect on either lamin A/C expression or localization (Vigouroux et al. 2001; Ostlund et al. 2001). The pathogenetic mechanism of inherited lipodystrophies is not yet clear; lamin A/C may be more directly involved in the formation, stabilization or regulation of transcription complexes involving SREBP proteins. Mutations in lamin A/C that affect this interaction may disrupt SREBP1 function, thus interfering with the differentiation of adipocytes. Mutation in lamin A/C reduces the amount of the DNA-bound adipocyte transcription factor SREBP1 and lowers the peroxisome proliferator-activated receptor expression, causing the impairment of pre-adipocyte differentiation (Maraldi et al. 2007). It has been suggested that the mutation in lamin A/C which leads to the FPLD may disrupt normal interaction between lamins and SREBPs at the nuclear membrane (Lloyd et al. 2002; Nikolova et al. 2004). Human emerin is a serine-rich protein of 254 amino acids (Bione et al. 1994). The sequence of emerin is composed of an N-terminal globular domain of about 50 residues, followed by a poly-Ser segment, then a region of 100 residues rich in hydrophobic amino acids comprising the nuclear localization signal (Ostlund et al. 1999; Tsuchiya et al. 1999), again a poly-Ser segment, and finally a C-terminal transmembrane region. Emerin has been shown to play a role of molecular sensor, which senses the increase in lamin A/C levels at the onset of adipogenesis. Emerin and lamin A/C have been shown to co-localize in cells (Manilal et al. 1998) and tissues (Manilal et al. 1999) and to interact directly with each other (Clements et al. 2000). Moreover,

Fig. 1 Native structure of lamin A/C in cartoon model and mutation site Arg482 in stick model

emerin-null fibroblasts have been reported to show increased β-catenin activity and peroxisome proliferator-activated receptor accumulation in the nucleus (Tilgner et al. 2009). Emerin appears to be involved in regulation of nuclear positioning and mechanosignaling transduction (Maraldi et al. 2011). It is found that mutation in lamin A/C caused mislocalization of emerin away from the nuclear periphery and responsible for skeleton and cardiac muscular dystrophies (Bank et al. 2011).

Conformational flexibility of a protein molecule affects its interaction with ligand and its biological partners at different level (Purohit et al. 2008; Purohit and Sethumadhavan 2009; Purohit et al. 2011a, b). In this report, dynamic behavior of lamin A/C protein is studied with the help of docking and molecular dynamics simulation in order to understand the structural changes involved in causing FPLD. The first objective of the current report is to address the effect of mutation (R482W) on interaction of lamin A/C with their biological partners as emerin and SREBP1. Second is, to address the unsolved structural issues of lamin A/C mutant responsible for FPLD. Third is, to correlate the structural changes to its function on mutation.

In this study we found that Mutant lamin A/C interacts with emerin and SREBP1 with more affinity than with native. Docking studies clearly show that the mutation R482W at lamin A/C worked as a gain-of-function mutation. Molecular dynamics simulation indicates the more atomic flexibility in mutant lamin than in the native.

Materials and methods

Datasets

We selected crystal structures of native lamin A/C (PDB ID 1IFR; Dhe-Paganon et al. 2002), Mutant lamin A/C (PDB ID 3GEF; Magracheva et al. 2009), emerin (PDB ID 1JEI; Wolff et al. 2001) and SREBP1 (PDB ID 1AM9; Párraga et al. 1998) from Brookhaven Protein Data Bank (Berman et al. 2000) for our investigation. We used monomer structure of lamin A/C (native/mutant), emerin and SREBP1 for docking simulation. The crystal structure of native lamin A/C, Mutant lamin A/C and SREBP1 were solved by X-ray diffraction method while, emerin structure was solved by NMR solution method. Out of ten models which is present in emerin PDB file the first model structure was used for analysis, since it is close to the average structure.

Protein–protein interaction analysis

The HADDOCK protocol (Dominguez et al. 2003; de Vries et al. 2010) was used to dock the lamin A/C (native/mutant) structures with their partners: Emerin and SREBP1. HADDOCK is a series of scripts that run in combination with ARIA (Nilges 1995; Nilges et al. 1997) and CNS (Brünger et al. 1998). The docking process in HADDOCK is driven by ambiguous interaction restraints (AIRs), which are derived from the available experimental information on the residues involved in the intermolecular interaction. Based on other studies of the interface surface residues in lamin A/C (position number 481, 483, 487, 514 and 520) together with interface residues on the partner proteins (residues between 36 and 44 on emerin and residues between 337 and 374 on SREBP1) were used as active residues and residues neighboring the active residues were used as passive residues (Sakaki et al. 2001; Lloyd et al. 2002; Clements et al. 2000).

At the first stage of the docking protocol (see also the HADDOCK website at http://www.nmr.chem.uu.nl/haddock), consisting of randomization of orientations and rigid body energy minimization, we have calculated 1,000 complex structures. The 200 solutions with the lowest intermolecular energies have been selected for semi-flexible simulated annealing in torsion angle space. The resulting structures have been then refined in explicit water. Finally, the solutions have been clustered using a threshold value of 1.5 Å for the pairwise backbone RMSD at the interface, and the resulting clusters have been ranked according to their average interaction energy (defined as the sum of van der Waals, electrostatic and AIRs energy terms) and buried surface area. One lowest energy structure of the lowest intermolecular energy cluster was selected for analysis. This lowest energy structure displayed no AIR restraint violations (within a threshold of 0.3 Å) and was accepted as the final docked structure for the complex. HADDOCK scoring is performed according to the weighted sum (HADDOCK score) of different energy terms which includes van der Waals energy, electrostatic energy, distance restraints energy, direct RDC restraint energy, intervector projection angle restraints energy, diffusion anisotropy energy, dihedral angle restraints energy, symmetry restraints energy, binding energy, desolvation energy and buried surface area. Along with HADOCK score and total interaction energy, we reported van der Waals energy, electrostatic energy, restraints violation energy, desolvation energy and buried surface area. Intermolecular contacts (hydrogen bonds and non-bonded contacts) were analyzed with DIMPLOT, which is part of the LIGPLOT software (Wallace et al. 1995). Using the default settings (3.9 Å heavy-atoms distance cut-off for non-bonded contacts; 2.7 and 3.3.5 Å proton–acceptor and donor–acceptor distance cut-offs, respectively, with minimum 90° angles (D–H–A, H–A–AA, D–A–AA) for hydrogen bonds) (McDonald and Thornton 1994).

Molecular dynamics simulation

Molecular dynamics simulations were performed using the GROMACS 4.0.5 (Hess et al. 2008; Spoel et al. 2005) running on a single 2.8 GHz Pentium IV IBM machine with 512 MB RAM and running Fedora Core 2 Linux package and GROMOS96 (Gunsteren et al. 1996) 43a1 force field implemented on LINUX architecture. Monomer structure of native and Mutant lamin A/C was used as starting point for MD simulations. The protein was solvated in a cubic 1.0 nm of 21,668 SPC (Berendsen et al. 1981) water molecules. At physiological pH, the protein is positively charged, thus in order to make the simulation system electrically neutral, we added chloride ions (Cl^-) to the simulation box using the "genion" tool that accompanies Gromacs. The systems were subjected to energy minimization for 1,000 steps by steepest descent. The minimized systems were then subjected to MD simulations in two steps. Initially, we performed under an NVT ensemble (constant number of particles, volume, and temperature) for 500 ps, followed by under an NPT ensemble (constant number of particles, volume, and temperature) for 1,000 ps each at 300 K with positions restrained for the entire system, except the water molecules, in order to ensure a balance of the solvent molecules around the residues of the protein. The well-equilibrated systems (with respect to pressure and density over the time) were then subjected to molecular dynamics simulations for 6 ns each at 300 K without any restriction. In all simulations, the temperature was kept constant at 300 K with a Berendsen thermostat (Berendsen et al. 1984). The particle mesh Ewald method (Essmann et al. 1995) was used to treat long-range Coulombic interactions and the simulations performed using the SANDER module (Case et al. 2002). The ionization states of the residues were set appropriate to pH 7 with all histidines assumed neutral. The SHAKE algorithm was used to constrain bond lengths involving hydrogens, permitting a time step of 2 fs. Van der Waals and coulomb interactions were truncated at 1.0 nm. The non-bonded pair list was updated every 10 steps and conformations were stored every 0.5 ps. Other analyses were performed using scripts included with the Gromacs (Hess et al. 2008) distribution.

The trajectory files were analyzed through the use of g_rms, g_gyrate, g_sas and g_rmsf of GROMACS utilities in order to obtain the root-mean-square deviation (RMSD), radius of gyration (Rg), solvent-accessible surface area (SASA) and root-mean square fluctuation (RMSF) value. Number of distinct hydrogen bonds formed by specific residues to other amino acids within the protein during the simulation (NH bond) were calculated using g_hbond. NH bond determined on the basis of donor–acceptor distance smaller than 0.35 nm and of donor–hydrogen-acceptor angle larger than 150°. Moreover, VMD (Humphrey et al. 1996) and Coot (Emsley and Cowtan 2004) packages were used for trajectory analysis and for the management of the simulation snapshot structures. The major focus of this study is to compare the dynamic behavior of wild and mutant proteins at 300 K. To that end we compare RMSF of carbon alpha, RMSD of backbone structure, Rg and SASA of protein between the trajectories generated at 300 K to investigate the flexible nature of mutants. In order to generate the three-dimensional backbone RMSD, Rg, SASA and RMSF of carbon-alpha carbon and motion projection of the protein in phase space of the system were plotted for all three simulations using ORIGIN program (version 6.0).

Principle component analysis

The calculation of the eigenvectors and eigenvalues, and their projection along the first two principal components, was carried out using essential dynamics (ED) method according to protocol (Amadei et al. 1993) within the GROMACS software package (Hess et al. 2008). The principle component analysis or ED is a technique that reduces the complexity of the data and extracts the concerted motion in simulations that are essentially correlated and presumably meaningful for biological function (Amadei et al. 1993). In the ED analysis, a variance/covariance matrix was constructed from the trajectories after removal of the rotational and translational movements. A set of eigenvectors and eigenvalues was identified by diagonalizing the matrix. The eigenvalues represented the amplitude of the eigenvectors along the multidimensional space, and the displacement of atoms along each eigenvector showed the concerted motions of protein along each direction. An assumption of ED analysis is that the correlated motions for the function of the protein are described by eigenvectors with large eigenvalues. The movements of protein in the essential subspace were identified by projecting the Cartesian trajectory coordinates along the most important eigenvectors from the analysis. For the simulation of both native and mutant only Ca atoms were included in the definition of the covariance matrices for the protein. The trajectory files were analyzed through the use of g_covar and g_anaeig of GROMACS utilities in order to perform ED.

Result and discussion

Traditional in silico docking approaches rely on defining the interface of complexes based on the surface geometry complementarity and amino acid pairwise affinities of the 3D structure of the unbound molecules without a prior

inclusion of any experimental information (Halperin et al. 2002; Janin et al. 2003). If used, experimental information is typically included posterior to filter solutions. HADDOCK, however, is a new method that directly allows incorporation of biological and/or biophysical information to drive docking (Dominguez et al. 2003). Docking with HADDOCK resulted in a cluster of structures with an overall backbone RMSD of 1.5 Å. The lowest energy structure produced during the run belongs to this cluster of structures and was consistent with the orientation of the manually docked structure (deviation of <20°). This lowest energy structure displayed no AIR restraint violations (within a threshold of 0.3 Å) and was accepted as the final docked structure for the complex.

In our paper we called native lamin A/C–emerin complex as complex I, Mutant lamin A/C–emerin complex as complex II, native lamin A/C–SREBP1 complex as complex III and Mutant lamin A/C–SREBP1 complex as complex IV and it is depicted in Fig. 2a–d. In-depth analysis of the docked complex reveals notable features. Calculation of interaction energy is very important to understand the affinity level of biological partners. Overall interaction energy of the complex mainly contributes to van der Waals and electrostatic interaction energy between lamin A/C (native and mutant) and emerin and SREBP1 protein. In the complex II, there were a significant contribution of van der Waals and electrostatic energy, -310.5 ± 60.1 and -46.2 ± 4.0 kcal/mol, respectively. The total protein–protein interaction energy of complex II was -447.81 kcal/mol. Van der Waals and electrostatic energy confirms significant amount of surface complementarities between Mutant lamin A/C and emerin in complex II. On the contrary, complex I has more van der Waals and electrostatics energies of -211.5 ± 44.7 and -38.6 ± 4.5 kcal/mol, respectively, and total interaction energy -247.21 kcal/mol when compared to the complex II. In similar manner complex IV exhibited total interaction energy of -227.61 kcal/mol and complex III exhibited total interaction energy of -159.04 kcal/mol. Less interaction has been found in complex III when compared to complex IV and this was due to less contribution of van der Waals and electrostatic energy in complex formation and this is depicted in Table 1. More negative value of interaction energy of complex II and complex IV indicates high affinity towards their biological partners (emerin and SREBP1) when compared to complex I and complex III. Estimates of van der Waals interaction energy were computed to provide a theoretical quantitative assessment of the protein–protein non-bonded interactions.

Buried surface area (BSA) is a measure of protein surface which is not exposed to water; more BSA indicates tighter biomolecular complex. In Table 1, complex II showed maximum BSA of $1{,}436.8 \pm 53.4$ Å^2, complex I showed minimum BSA of $1{,}219.5 \pm 80.1$ Å^2 and complex III and complex IV showed intermediate BSA. Consideration of desolvation component (the loss of interactions with the water phase) is important because it overcompensates the interaction energy and results in an opposite effect (Teng et al. 2009; Zhang et al. 2011). Desolvation energy, restraints violation energy and BSA have good correlation with docking score and interaction energy of complex during docking simulation (Table 1). Major difference between docking score, interaction energy and BSA were observed in all the complexes. The net values of complex I and II is significantly higher than complex III and IV, this indicates that the effect of gain-of-function mutation in lamin A/C enables more tight binding with emerin when compared to SREBP1 (Table 1).

Hydrogen bonds and slat bridges are by far the most important specific interactions in biological recognition processes. The number of intermolecular hydrogen bonds and slat bridges are calculated for all complexes; it is depicted in Fig. 3 and Table 2. The presence of salt-bridge is an evidence of close proximity in the structure. Complex II has shown 11 hydrogen bonds and four salt-bridges while complex III has shown 8 hydrogen bonds and 2 salt-bridges. Complex IV has shown 9 and one salt-bridge which has distance of 2.11 Å while, complex I has shown 8 hydrogen bonds and one salt-bridge which has distance of 3.01 Å. Studies have shown that the single best structural parameter correlating with binding affinity is the amount of hydrophobic surface buried upon ligand binding (Young et al. 1994; Eisenhaber and Argos 1996; Vallone et al. 1998). In Fig. 3, complex I showed 16 residues while complex II showed only 10 residues involved in hydrophobic interaction. In a similar manner complex III showed 15 residues while, complex IV showed 14 residues participating in hydrophobic interactions. It further indicates the tight atomic contacts of Mutant lamin A/C with emerin and SREBP1 as compared to native lamin A/C.

Protein–protein docking analysis and intermolecular hydrogen bonding patterns indicates that the mutation (R482W) in lamin A/C increases its affinity towards emerin and SREBP1. Since, the docking process solely depends on the location of binding residues (active residues) on the protein surface, it proves that deviation from actual position of binding residues (position number 481, 483, 487, 514 and 520) of Mutant lamin A/C may be the reason for tight binding with emerin and SREBP1 when compared to native lamin A/C. The three factors namely, score difference in docking process, variation in interaction energy and variation in buried surface of complex probably correspond to conformational alteration of protein-binding surface due to mutation.

MD simulations were carried out with structures to get conformational fluctuations of native and Mutant lamin

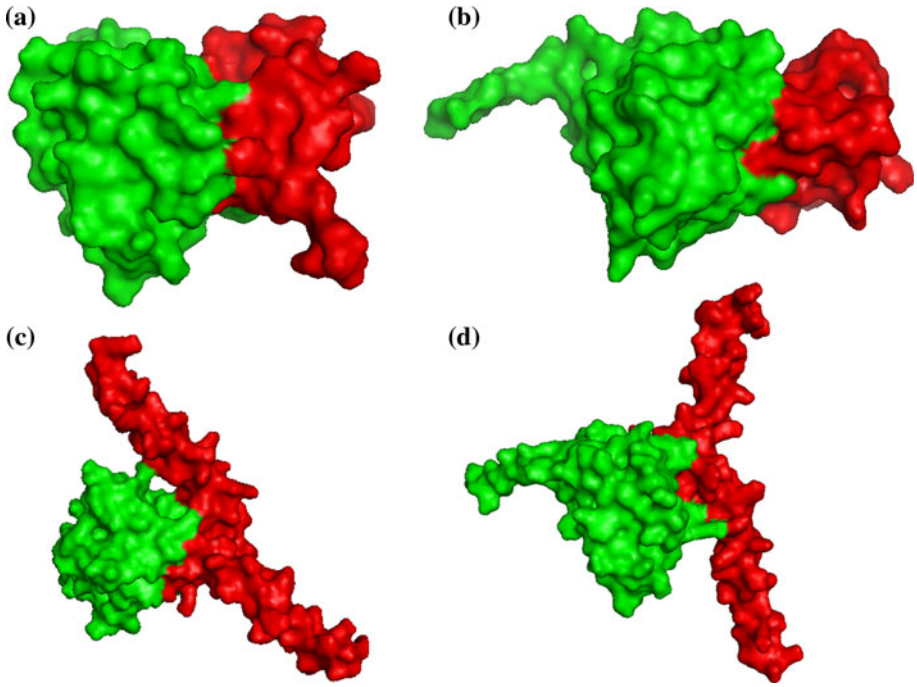

Fig. 2 Surface representation of Lamin A/C complex: **a** complex I, **b** complex II, **c** complex III and **d** complex IV. The symbol coding scheme is as follows: Lamin A/C (native/mutant) in *green* color and emerin/SREBP1 in *red* color (color figure online)

Table 1 Statistical analysis of protein–protein docking result obtained by HADDOCK

Lamin A/C complex	HADDOCK score	Total Interaction energy (Kcal mol^{-1})	Van der Waals energy (Kcal mol^{-1})	Electrostatic energy (Kcal mol^{-1})	Desolvation energy (Kcal mol^{-1})	Restraints violation energy (Kcal mol^{-1})	Buried surface area ($Å^2$)
Complex I	−65.0 ± 6.5	−247.21	−38.6 ± 4.5	−211.5 ± 44.7	−6.7 ± 2.4	29.5 ± 36.81	1,219.5 ± 80.1
Complex II	−100.1 ± 11.6	−447.81	−46.2 ± 4.0	−310.5 ± 60.1	−19.8 ± 7.0	65.6 ± 30.34	1,436.8 ± 53.4
Complex III	−72.0 ± 5.6	−159.04	−43.9 ± 4.2	−138.1 ± 12.7	−9.4 ± 4.3	43.4 ± 38.33	1,230.5 ± 93.6
Complex IV	−83.0 ± 5.2	−227.61	−47.0 ± 4.2	−179.8 ± 27.1	−11.7 ± 5.1	58.3 ± 24.61	1,338.4 ± 33.0

A/C. We have highlighted RMSF of C-alpha carbon of binding residues by trajectory analysis obtained by MD simulation. Distinct NH bond analysis was performed to understand the flexibility behavior of residues. In order to verify the system stabilized along the MD simulations, we have showed the plot of energy × time for the MD simulations (Fig. 4).

We calculated the RMSD for all the Cα atoms from the initial structure, which were considered as a central criterion to measure the convergence of the protein system concerned (Fig. 5). In Fig. 5, native and Mutant lamin A/C protein showed similar fashion of deviation till 255 ps from their starting structure, resulting in a backbone RMSD of ∼0.1 to 0.13 nm during the simulations, this deviation in mutant only persists till 255 ps from starting structure but after this, the mutant showed more deviation and attained approximately ∼0.20 nm of backbone RMSD at 1,400 ps while native structure maintained RMSD value of ∼0.11 to 0.13 nm. Between periods of 1,400–5,500 ps, native structure showed deviation between 0.15 and 0.16 nm and attained RMSD value of ∼0.20 nm at 5,200 ps. The mutant retained maximum deviation till end and around the period of 5,400 ps it attain RMSD value of ∼0.25 nm. From their starting structure, the wild structure deviated minimum but mutant exhibited maximum deviation. This magnitude of fluctuations, together with very small difference between the average RMSD values after the relaxation period (∼0.13 nm), led to the conclusion that the simulations produced stable trajectories, thus providing a suitable basis for further analyses.

The Rg is defined as the mass-weighted root mean square distance of a collection of atoms from their common center of mass. Hence, this analysis gives us insight into the overall dimensions of the protein. The plot of radius of gyration of Cα atoms of the protein versus time at 300 K is shown in Fig. 6. We observed the major fluctuation in both native and mutant between 0 and 6,000 ps. In the native structure the value of Rg ∼1.28 nm at 0 ps, ∼1.28 nm at

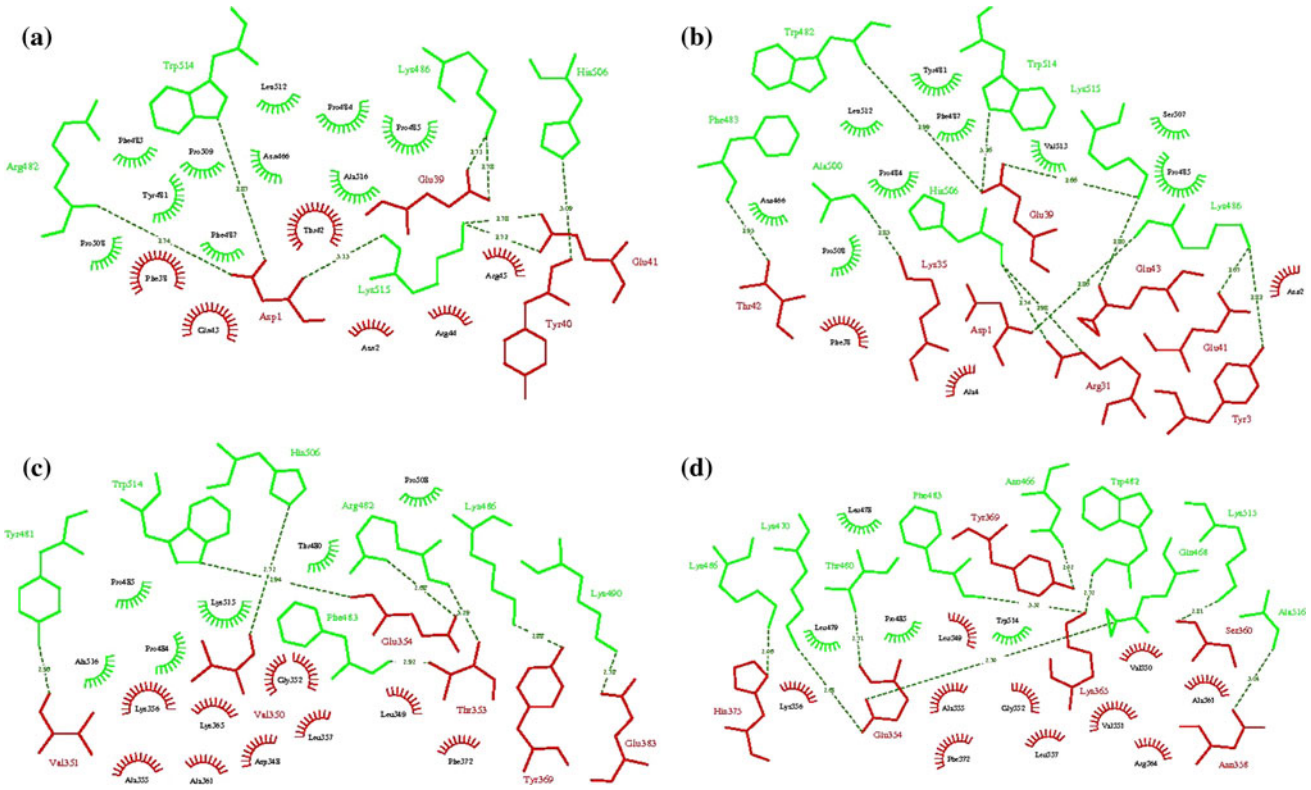

Fig. 3 Residual interactions at protein–protein interface in Lamin A/C complex: **a** complex I, **b** complex II, **c** complex III and **d** complex IV. The symbol coding scheme is as follows: Lamin A/C (native/mutant) in *green* color, emarin/SREBP1 in *red* color. Hydrogen bonding interactions are denoted by *dashed lines*. Residues involved in the hydrophobic interactions are shown as starbursts. This illustration was prepared by Ligplot (color figure online)

Table 2 Slat bridges and their distance in lamin A/C complex

Lamin A/C complex	Atom, residue and residue number	Distance (Å)
Complex I	NZ LYS 486–OE1 GLU 39	2.78
	NZ LYS 515–OE1 GLU 41	2.72
Complex II	NZ LYS 486–OD1 ASP 1	2.78
	NZ LYS 486–OD2 ASP 1	3.00
	NZ LYS 486–OE1 GLU 41	3.85
	NZ LYS 515–OE1 GLU 39	2.66
Complex III	NZ LYS 490–OE1 GLU 383	3.01
Complex IV	NZ LYS 490–OE1 GLU 383	2.11

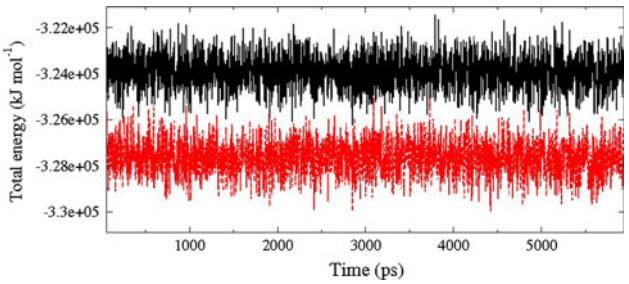

Fig. 4 Plot of total energy as a function of time for the MD simulations. The symbol coding scheme is as follows: native (*solid line in black*) and mutant (*dashed line in red*) (color figure online)

650 ps, 1.29 nm at 2,422 ps, 1.28 nm at 4,290 ps, 1.28 nm at 5,555 ps and 1.28 nm at 6,000 ps while, mutant structure showed the value of Rg ~1.28 nm at 0 ps, ~1.31 nm at 650 ps, 1.32 nm at 2,422 ps, 1.30 nm at 4,290 ps, 1.30 nm at 5,555 ps and 1.29 nm at 6,000 ps. Native curve do not differ significantly and maintain the values of Rg ~1.27 to 1.29 nm, indicating that the native conformation is largely preserved throughout the simulation time. Mutant structure showed large fluctuation in Rg that is between ~1.28 and 1.33 nm. The average value of Rg during simulation time period in native and mutant is indicated in Table 3.

The change of SASA of the native and mutant protein with time is shown in Fig. 7. Mutant protein indicated greater values of SASA with time while, native showed smaller values of SASA with time. The average value of SASA during the simulation time period in native and mutant is indicated in Table 3. The large fluctuation in the radius of gyration in the mutant indicated that the protein might be undergoing a significant structural transition. This was also supported by the fluctuations in solvent-accessible surface areas (Fig. 7). In contrast, judging from the stable curves for the radius of gyration and solvent-accessible

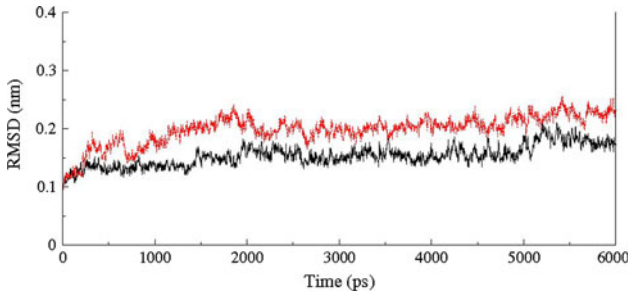

Fig. 5 Time evolution of backbone RMSDs are shown as a function of time of the native and Mutant lamin A/C structures at 300 K. The symbol coding scheme is as follows: native (*solid line in black*) and mutant (*dashed line in red*) (color figure online)

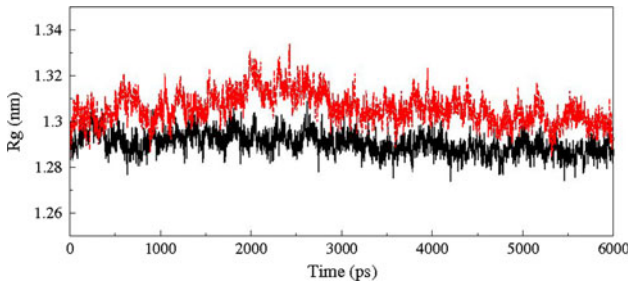

Fig. 6 Radius of gyration of Cα atoms of native and Mutant lamin A/C versus time at 300 K. The symbol coding scheme is as follows: native (*solid line in black*) and mutant (*dashed line in red*) (color figure online)

Table 3 Average values of Rg, SASA and average number of protein–protein H-bonds in native and Mutant lamin A/C protein

	Native lamin A/C	Mutant lamin A/C
aRg	1.28	1.3
aSASA	38.32	41.63
Protein–solvent H-bonds	270.55	254.74

The values of Rg and SASA are given in nm

Rg radius of gyration, *SASA* solvent-accessible surface area, *H-bonds* hydrogen bonds

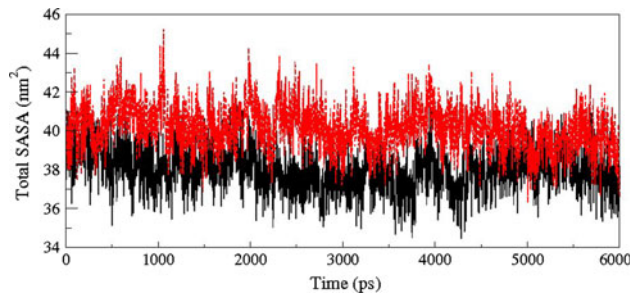

Fig. 7 Solvent-accessible surface area (*SASA*) of native and Mutant lamin A/C versus time at 300 K. The symbol coding scheme is as follows: native (*solid line in black*) and mutant (*dashed line in red*) (color figure online)

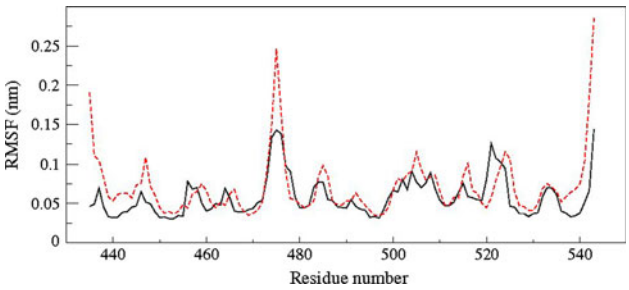

Fig. 8 RMSF of the backbone CAs of Cα atoms of native and Mutant lamin A/C versus time at 300 K. The symbol coding scheme is as follows: native (*solid line in black*) and mutant (*dashed line in red*) (color figure online)

Table 4 C-alpha carbon root mean square mean fluctuation (in nm) of binding residues of native and Mutant lamin A/C

Lamin A/C protein	RMSF of C-alpha carbon atom of binding residues (in nm)				
	481	483	487	512	520
Native	0.04	0.06	0.05	0.05	0.04
Mutant (R482W)	0.05	0.08	0.07	0.06	0.08

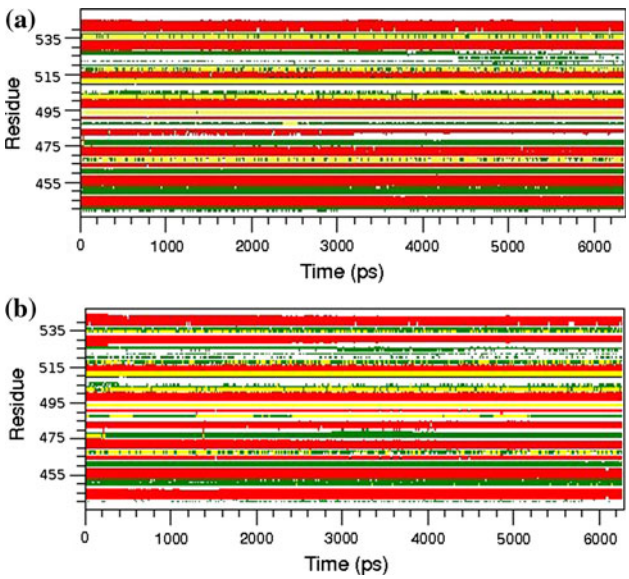

Fig. 9 Time evolution of the secondary structural elements of the protein at 300 k (DSSP classification). **a** Native lamin A/C and **b** Mutant lamin A/C

surface areas, major structural transition occurred between 2,000 and 4,000 ps in native and mutant proteins.

A more detailed picture of differences in residue mobility within and between simulations can be obtained from graphs of the RMSF of Cα atoms relative to the

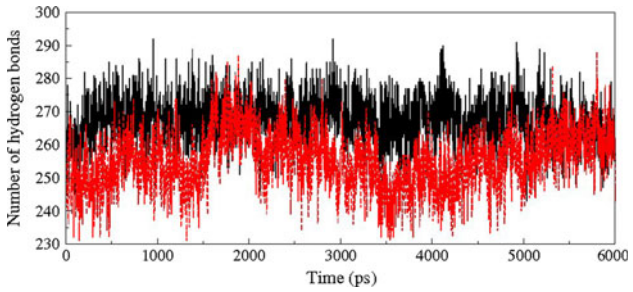

Fig. 10 Average number of protein–solvent intermolecular hydrogen bonds in native and Mutant lamin A/C versus time at 300 K. The symbol coding scheme is as follows: native (*solid line in black*) and mutant (*dashed line in red*) (color figure online)

average structure and it is shown in Fig. 8. The regions of greater flexibility correspond to the termini of the proteins and also in the loop regions. Mutant lamin exhibited more flexibility compared to native lamin protein. To investigate the flexible behavior of binding residues, we plotted the RMSF of Cα atoms between the residues of 480–520 where the binding residues of lamin locate. In Mutant lamin A/C, binding residues exhibited highest degree of fluctuation compared to native lamin and it is depicted in Table 4.

Additional information on the structural flexibility of lamin proteins is obtained by the analysis of time-dependent secondary structure fluctuations. Figure 9a, b shows the secondary structural elements as a function of simulation time. Figure 9a reveals that β-sheets, coil, bends and turns are observed in both native and mutant protein during simulation time period. In native lamin, first few residues between positions of 435–455 appeared as β-sheets and bends with few coil conformation till the end of the simulation but in mutant lamin this region shows β-sheets and bends with more traces of coil conformation. Compared to native lamin, mutant lamin showed significant structural changes between a region of residues 470–495 during simulation. Between residues 475–485, native lamin showed more coil–coil conformation than mutant. In native structure the coil conformation at 3,000 ps slowly appeared in bend conformation in mutant lamin. Between residues of

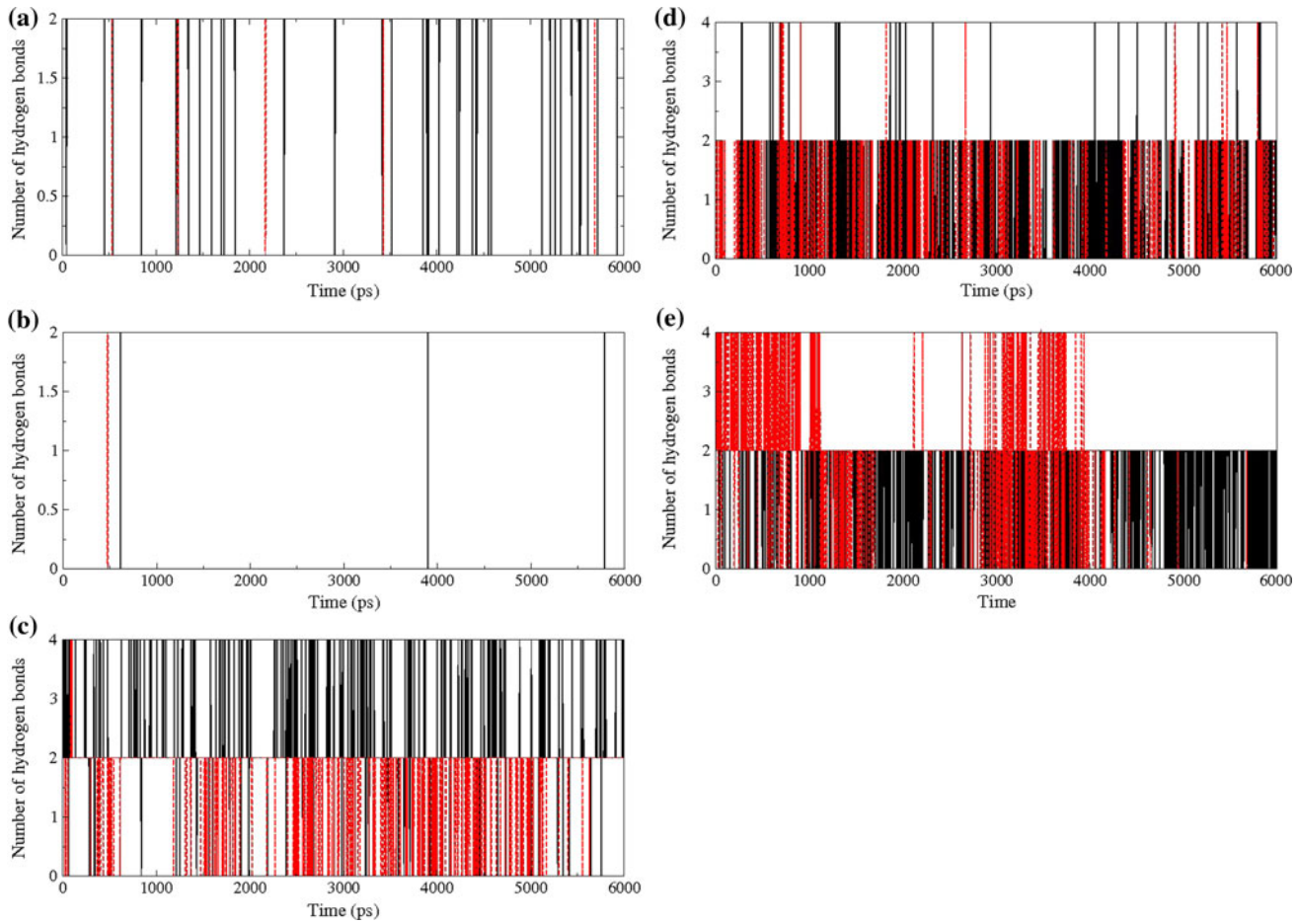

Fig. 11 Time evolution of number of distinct intramolecular hydrogen bonds of amino acid at position: **a** 481, **b** 483, **c** 487, **d** 514 and **e** 520 of native and mutant to other amino acids within the protein during the simulations. The symbol coding scheme is as follows: native (*solid line in black*) and mutant (*dashed line in red*) (color figure online)

485–490 bends change to turns conformation in mutant lamin. There were no significant changes observed between residues of 495–515 in native and mutant lamin except a few bend conformation changes to coil conformation near to residues at 505th. After residues of 515th till end, in mutant lamin bend conformations were dominated over coil and turn conformations.

Intermolecular NH bond is calculated for native and mutant structure during the simulation time. Notable differences in protein–solvent interactions are evident in native and mutant and it is shown in Fig. 10. More intermolecular NH bond in native structure might help to maintain its rigidity while less tendency of the mutant to involve in participating in hydrogen bonding with solvent makes it more flexible (Table 3).

Distinct intramolecular NH bond analysis of residues at positions 481, 483, 487, 514 and 520 of mutant has shown hydrogen bonds 0–2 (less frequent), 0–2 (less frequent), 0–2, 0–2 and 0–4, respectively while, in native it has 0–2 (more frequent), 0–2 (more frequent), 0–4, 0–4 and 0–2 hydrogen bonds with surrounding residues, respectively (Fig. 11). 481, 483, 487 and 514 have shown more degree of flexibility in mutant and less in native lamin A/C (Table 4). The alteration in flexibility was validated by intramolecular NH bond analysis at binding residues. In Mutant lamin A/C, the binding residues exhibited more flexibility and have shown less participation in H-bonding with other amino acids, while native lamin A/C residues were rigid and have more H-bonds. On the basis of RMSF observation and NH bond analysis, it is confirmed that the occurrence of the mutation leads to a more flexible binding site due to the formation of less hydrogen bonds. The flexible nature of binding residues of mutant makes it more available for interaction with emerin and SREBP1 protein, in turns it provide more docking score (Table 1).

A better view of dynamical mechanical properties of the investigated system has been obtained by using essential dynamics (ED) analysis. To further support our MD simulation result, the large-scale collective motions of the native and mutant protein using ED analysis were determined. The dynamics of two proteins is best achieved via characterization of its phase space behavior. The eigenvectors of the covariance matrix are called its principle components. The change of particular trajectory along each eigenvector was obtained by this projection.

The spectrum of the corresponding eigenvalues (Fig. 12a) indicates that the fluctuation of the system is basically confined within the first two eigenvectors. The projection of trajectories obtained at 300 K onto the first two principal components (PC1, PC2) shows the motion of two proteins in phase space (Fig. 12a). On these projections, we see clusters of stable states. Two features are very apparent from these plots. Firstly, the clusters are well

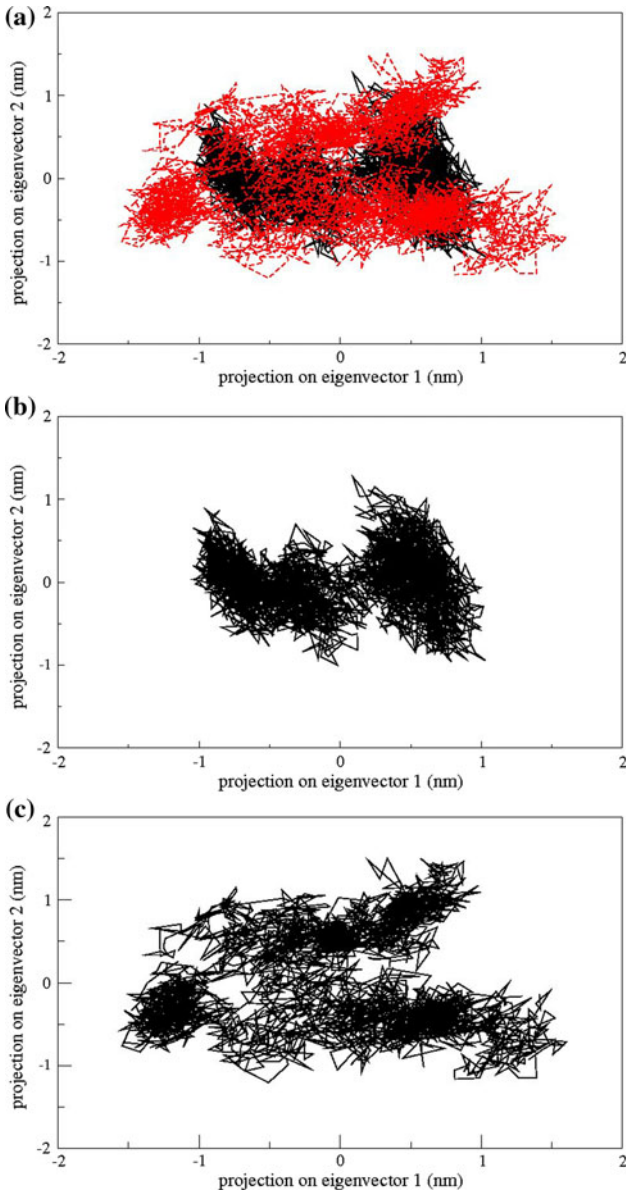

Fig. 12 Projection of the motion of the protein in phase space along the first two principal eigenvectors at 300 K: **a** native (*solid line in black*) and mutant (*dashed line in red*). For clarity's sake, each trajectory projection is also shown separately in **b**, **c** (color figure online)

defined in native than mutant. Secondly, mutant covers a larger region of phase space particularly along PC1 plane than native and it is depicted in Fig. 12a. Our observation thus corroborates with the idea of higher flexibility of mutant than native at 300 K. The overall flexibility of two proteins has been calculated also by the trace of the diagonalized covariance matrix of the Cα atomic positional fluctuations. We have obtained the following values for native protein 1.32 nm^2 and mutant protein 3.69 nm^2 again confirming the overall increased flexibility of mutant than native at 300 K.

Conclusion

How mutations in lamin A/C protein result in many different disease phenotypes remains poorly understood. In this report, we emphasized the consequences of R482W mutation of lamin A/C which causes FPLD. Intermolecular interactions between native and Mutant lamin A/C with emerin and SREBP1 were observed. The Mutant lamin A/C showed more protein–protein interaction (with emerin and SREBP1) when compared to native lamin A/C (with emerin and SREBP1). Conformational perturbation in lamin A/C was observed using classical MD simulations. Mutant form of lamin A/C showed more structure deviation and expanded conformation as compared to native. Due to these conformational changes, Mutant lamin A/C acquired more SASA and active residues which participated in the protein–protein interactions got misplaced from the original state and showed less interaction with emerin and SREBP1. With support of essential dynamics studies it is cleared that due to mutation, lamin A/C acquired more degree of flexibility in phase space. Studies on lamin A/C mutation through MD simulations and computer experiments clarify the pathogenic role of a specific point mutation. Our in silico investigation provides a clear-cut clue to wet lab scientists to understand cellular mechanisms underlying the disease.

Acknowledgments We gratefully acknowledge the management of Vellore Institute of Technology University for providing the facilities to carry out this work. We thank the anonymous reviewers for their helpful comments and critical reading of the manuscript.

Conflict of interest The authors declare that they have no competing interests.

References

Amadei A, Linssen ABM, Berendsen HJC (1993) Essential dynamics of proteins. Proteins 17:412–425

Araújo-Vilar D, Lattanzi G, González-Méndez B, Costa-Freitas AT, Prieto D, Columbaro M, Mattioli E, Victoria B, Martínez-Sánchez N, Ramazanova A, Fraga M, Beiras A, Forteza J, Domínguez-Gerpe L, Calvo C, Lado-Abeal J (2009) Site-dependent differences in both prelamin A and adipogenic genes in subcutaneous adipose tissue of patients with type 2 familial partial lipodystrophy. J Med Genet 46(1):40–48

Bank EM, Ben-Harush K, Wiesel-Motiuk N, Barkan R, Feinstein N, Lotan O, Medalia O, Gruenbaum Y (2011) A laminopathic mutation disrupting lamin filament assembly causes disease-like phenotypes in *Caenorhabditis elegans*. Mol Biol Cell 22(15): 2716–2728

Berendsen HJC, Postma JPM, Gunsteren WFV, Hermans J (1981) Interaction models for water in relation to protein hydration. In: Pullman B (ed) Intermolecular forces. D Reidel Publishing Company, Dordrecht, pp 331–342

Berendsen HJC, Postma JPM, DiNola A, Hakk JR (1984) Molecular dynamics with coupling to an external bath. J Chem Phys 81:3684–3690

Berman HM, Westbrook JZ, Feng G, Gilliland TN, Bhat H, Weissig IN et al (2000) Nucleic Acids Res 28:235–242

Bione S, Maestrini E, Rivella S, Mancini M, Regis S, Romeo G, Toniolo D (1994) Identification of a novel X-linked gene responsible for Emery–Dreifuss muscular dystrophy. Nat Genet 8:323–327

Brünger AT, Adams PD, Clore GM, DeLano WL, Gros P, Grosse-Kunstleve RW, Jiang JS, Kuszewski J, Nilges M, Pannu NS, Read RJ, Rice LM, Simonson T, Warren GL (1998) Crystallography and NMR system: a new software suite for macromolecular structure determination. Acta Crystallogr D Biol Crystallogr 54:905–921

Burke B, Stewart CL (2002) Life at the edge: the nuclear envelope and human disease. Nat Rev Mol Cell Biol 3:575–585

Burn J, Baraitser M (1986) Partial lipoatrophy with insulin resistant diabetes and hyperlipidaemia (Dunnigan syndrome). J Med Genet 23:128–130

Cao H, Hegele RA (2000) Nuclear lamin A/C R482Q mutation in Canadian kindreds with Dunnigan-type familial partial lipodystrophy. Hum Mol Genet 9:109–112

Case DA, Pearlman DA, Caldwell JW, Wang J, Ross WS, Simmerling CL, Darden TA, Mertz KM, Stanton RV, Cheng AL, Vincent JJ, Crowley M, Tsue V, Gohlke H, Radmer R, Duan Y, Pitera J, Massova I, Seibel GL, Singh C, Weiner P, Kollman PA (2002) AMBER simulation software package, version 7, vol 2006. University of California, San Francisco

Clements L, Manilal S, Love DR, Morris GE (2000) Direct interaction between emerin and lamin A. Biochem Biophys Res Commun 267:709–714

Cohen M, Lee KK, Wilson KL, Gruenbaum Y (2001) Transcriptional repression, apoptosis, human disease and the functional evolution of the nuclear lamina. Trends Biochem Sci 26:41–47

de Vries SJ, van Dijk M, Bonvin AMJJ (2010) The HADDOCK web server for data-driven biomolecular docking. Nat Protoc 5:883–897

Dhe-Paganon S, Werner ED, Chi YI, Shoelson SE (2002) Structure of the globular tail of nuclear lamin. J Biol Chem 277(20):17381–17384

Dominguez C, Boelens R, Bonvin AM (2003) HADDOCK: a protein–protein docking approach based on biochemical or biophysical information. J Am Chem Soc 125:1731–1737

Eisenhaber F, Argos P (1996) Hydrophobic regions on protein surfaces: definition based on hydration shell structure and a quick method for their computation. Protein Eng 9(12):1121–1133

Emsley P, Cowtan K (2004) Coot: model-building tools for molecular graphics. Acta Crystallogr Sect D Biol Crystallogr 60:2126–2132

Essmann U, Perera L, Berkowitz ML, Darden T, Lee H, Pedersen LG (1995) A smooth particle mesh Ewald method. J Chem Phys 103:8577–8593

Frock RL, Kudlow BA, Evans AM, Jameson SA, Hauschka SD, Kennedy BK (2006) Lamin A/C and emerin are critical for skeletal muscle satellite cell differentiation. Genes Dev 20(4): 486–500

Garg A, Peshock RM, Fleckenstein JL (1999) Adipose tissue distribution pattern in patients with familial partial lipodystrophy (Dunnigan variety). J Clin Endocrinol Metab 84:170–174

Gunsteren WFV, Billeter SR, Eising AA, Hunenberger PH, Kruger P, Mark AE, Scott WRP, Tironi TG (1996) Biomolecular simulation: the Gromos 96 manual and user guide. Hochschulverlag AG an der Zurich, Zurich

Halperin I, Ma B, Wolfson H, Nussinov R (2002) Principles of docking: an overview of search algorithms and a guide to scoring functions. Proteins Struct Funct Genet 47:409–443

Hegele RA (2001) Premature atherosclerosis associated with monogenic insulin resistance. Circulation 103:2225–2229

Hegele RA, Cao H, Anderson CM, Hramiak IM (2000a) Heterogeneity of nuclear lamin A mutations in Dunnigan-type familial partial lipodystrophy. J Clin Endocrinol Metab 85:3431–3435

Hegele RA, Anderson CM, Cao H (2000b) Lamin A/C mutation in a woman and her two daughters with Dunnigan-type partial lipodystrophy and insulin resistance. Diabetes Care 23:258–259

Hess B, Kutzner C, Spoel D, Lindahl E (2008) GROMACS 4: algorithms for highly efficient, load-balanced, and scalable molecular simulation. J Chem Theory Comput 4:435–447

Humphrey W, Dalke A, Schulten K (1996) VMD: visual molecular dynamics. J Mol Graph 14:33–38

Jacob KN, Garg A (2006) Laminopathies: multisystem dystrophy syndromes. Mol Genet Metab 87:289–302

Janin J, Henrick K, Moult J, Eyck LT, Sternberg MJ, Vajda S, Vakser I, Wodak SJ (2003) CAPRI: a critical assessment of predicted interactions. Proteins Struct Funct Genet 52:2–9

Kim JB, Spiegelman BM (1996) ADD1/SREBP1 promotes adipocyte differentiation and gene expression linked to fatty acid metabolism. Genes Dev 10(9):1096–1107

Kobberling J, Dunnigan MF (1986) Familial partial lipodystrophy: two types of an X linked dominant syndrome, lethal in the hemizygous state. J Med Genet 23:120–127

Lado-Abeal J, Calvo RM, Victoria B, Castro I, Obregon MJ, Araujo-Vilar D (2010) Regional decrease of subcutaneous adipose tissue in patients with type 2 familial partial lipodystrophy is associated with changes in thyroid hormone metabolism. Thyroid. 20(4):419–424

Lloyd DJ, Trembath RC, Shackleton S (2002) A novel interaction between lamin A and SREBP1: implications for partial lipodystrophy and other laminopathies. Hum Mol Genet 11:769–777

Magracheva E, Kozlov S, Stewart CL, Wlodawer A, Zdanov A (2009) Structure of the lamin A/C R482W mutant responsible for dominant familial partial lipodystrophy (FPLD). Acta Crystallogr Sect F Struct Biol Cryst Commun 65:665–670

Manilal S, Man NT, Morris GE (1998) Colocalization of emerin and lamins in interphase nuclei and changes during mitosis. Biochem Biophys Res Commun 249:643–647

Manilal S, Sewry CA, Pereboev A (1999) Colocalization of emerin and lamins in interphase nuclei and changes during mitosis. Hum Mol Genet 8:353–359

Maraldi NM, Capanni C, Mattioli E, Columbaro M, Squarzoni S, Parnaik WK, Wehnert M, Lattanzi G (2007) A pathogenic mechanism leading to partial lipodystrophy and prospects for pharmacological treatment of insulin resistance syndrome. Acta Biomed 78:207–215

Maraldi NM, Capanni C, Cenni V, Fini M, Lattanzi G (2011) Laminopathies and lamin-associated signaling pathways. J Cell Biochem 112(4):979–992

McDonald IK, Thornton JM (1994) Satisfying hydrogen bonding potential in proteins. J Mol Biol 238:777–793

Newport JW, Wilson KL, Dunphy WG (1990) A lamin-independent pathway for nuclear envelope assembly. J Cell Biol 111:2247–2259

Nikolova V, Leimena C, McMahon AC, Tan JC, Chandar S, Jogia D, Kesteven SH, Michalicek J, Otway R, Verheyen F, Rainer S, Stewart CL, Martin D, Feneley MP, Fatkin D (2004) Defects in nuclear structure and function promote dilated cardiomyopathy in lamin A/C-deficient mice. J Clin Invest 113(3):357–369

Nilges M (1995) Calculation of protein structures with ambiguous distance restraints. Automated assignment of ambiguous NOE crosspeaks and disulphide connectivities. J Mol Biol 245:645–660

Nilges M, Macias MJ, O'Donoghue SI, Oschkinat H (1997) Automated NOESY interpretation with ambiguous distance restraints: the refined NMR solution structure of the pleckstrin homology domain from beta-spectrin. J Mol Biol 269:408–422

Ostlund C, Ellenberg J, Hallberg E, Lippincott-Schwartz J, Worman HJ (1999) Intracellular trafficking of emerin, the Emery–Dreifuss muscular dystrophy protein. J Cell Sci 112:1709–1719

Ostlund C, Bonne G, Schwartz K, Worman HJ (2001) Properties of lamin A mutants found in Emery–Dreifuss muscular dystrophy, cardiomyopathy and Dunnigan-type partial lipodystrophy. J Cell Sci 114:4435–4445

Párraga A, Bellsolell L, Ferré-D'Amaré AR, Burley SK (1998) Co-crystal structure of sterol regulatory element binding protein 1a at 2.3 A resolution. Structure 6(5):661–672

Prokocimer M, Davidovich M, Nissim-Rafinia M, Wiesel-Motiuk N, Bar DZ, Barkan R, Meshorer E, Gruenbaum Y (2009) Nuclear lamins: key regulators of nuclear structure and activities. J Cell Mol Med 13:1059–1085

Purohit R, Sethumadhavan R (2009) Structural Basis for the resilience of darunavir (TMC114) resistance major flap mutations of HIV-1 protease. Interdiscip Sci 1(4):320–328

Purohit R, Rajasekaran R, Sudandiradoss C, George Priya Doss C, Ramanathan K, Sethumadhavan R (2008) Studies on flexibility and binding affinity of Asp25 of HIV-1 protease mutants. Int J Biol Macromol 42(4):386–391

Purohit R, Rajendran V, Sethumadhavan R (2011a) Relationship between mutation of serine residue at 315th position in *M. tuberculosis* catalase-peroxidase enzyme and isoniazid susceptibility: an in silico analysis. J Mol Model 17(4):869–877

Purohit R, Rajendran V, Sethumadhavan R (2011b) Studies on adaptability of binding residues and flap region of TMC-114 resistance HIV-1 protease mutants. J Biomol Struct Dyn 29(1):137–152

Sakaki M, Koike H, Takahashi N, Sasagawa N, Tomioka S, Arahata K, Ishiura S (2001) Interaction between emerin and nuclear lamins. J Biochem 129(2):321–327

Schmidt HH, Genschel J, Baier P, Schmidt M, Ockenga J, Tietge UJ, Pröpsting M, Büttner C, Manns MP, Lochs H, Brabant G (2001) Dyslipemia in familial partial lipodystrophy caused by an R482W mutation in the LMNA gene. J Clin Endocrinol Metab 86(5):2289–2295

Shackleton S, Lloyd DJ, Jackson SN, Evans R, Niermeijer MF, Singh BM, Schmidt H, Brabant G, Kumar S, Durrington PN, Gregory S, O'Rahilly S, Trembath RC (2000) LMNA, encoding lamin A/C, is mutated in partial lipodystrophy. Nat Genet 24:153–156

Speckman RA, Garg A, Du F, Bennett L, Veile R, Arioglu E, Taylor SI, Lovett M, Bowcock AM (2000) Mutational and haplotype analyses of families with familial partial lipodystrophy (Dunnigan variety) reveal recurrent missense mutations in the globular C-terminal domain of lamin A/C. Am J Hum Genet 66:1192–1198

Spoel D, Lindahl E, Hess B, Groenhof G, Mark AE, Berendsen HJ (2005) GROMACS: fast, flexible, and free. J Comput Chem 26:1701–1718

Strelkov SV, Herrmann H, Aebi U (2003) Molecular architecture of intermediate filaments. Bioessays 25:243–251

Stuurman N, Heins S, Aebi U (1998) Nuclear lamins: their structure, assembly, and interactions. J Struct Biol 122:42–66

Sullivan T, Escalante-Alcalde D, Bhatt H, Anver M, Bhat N, Nagashima K, Stewart CL, Burke B (1999) Loss of A-type lamin expression compromises nuclear envelope integrity leading to muscular dystrophy. J Cell Biol 147:913–920

Teng S, Madej T, Panchenko A, Alexov E (2009) Modeling effects of human single nucleotide polymorphisms on protein–protein interactions. Biophys J 96(6):2178–2188

Tilgner K, Wojciechowicz K, Jahoda C, Hutchison C, Markiewicz E (2009) Dynamic complexes of A-type lamins and emerin influence adipogenic capacity of the cell via nucleocytoplasmic distribution of {beta}-catenin. J Cell Sci 122:401–413

Tsuchiya Y, Hase A, Ogawa M, Yorifuji H, Arahata A (1999) Distinct regions specify the nuclear membrane targeting of emerin, the responsible protein for Emery–Dreifuss muscular dystrophy. Eur J Biochem 259:859–886

Vallone B, Miele AE, Vecchini P, Chiancone E, Brunori M (1998) Free energy of burying hydrophobic residues in the interface between protein subunits. Proc Natl Acad Sci USA 95:6103–6107

Vantyghem MC, Pigny P, Maurage CA, Rouaix-Emery N, Stojkovic T, Cuisset JM, Millaire A, Lascols O, Vermersch P, Wemeau JL, Capeau J, Vigouroux C (2004) Patients with familial partial lipodystrophy of the Dunnigan type due to a LMNA R482W mutation show muscular and cardiac abnormalities. J Clin Endocrinol Metab 89(11):5337–5346

Vantyghem MC, Faivre-Defrance F, Marcelli-Tourvieille S, Fermon C, Evrard A, Bourdelle-Hego MF (2007) Familial partial lipodystrophy due to the LMNA R482W mutation with multinodular goitre, extrapyramidal syndrome and primary hyperaldosteronism. Clin Endocrinol (Oxf) 67(2):247–249

Vigouroux C, Magré J, Vantyghem MC, Bourut C, Lascols O, Shackleton S, Lloyd DJ, Guerci B, Padova G, Valensi P, Grimaldi A, Piquemal R, Touraine P, Trembath RC, Capeau J (2000) Lamin A/C gene. Sex-determined expression of mutations in Dunnigan-type familial partial lipodystrophy and absence of coding mutations in congenital and acquired generalized lipoatrophy. Diabetes 49:1958–1962

Vigouroux C, Auclair M, Dubosclard E, Pouchelet M, Capeau J, Courvalin JC, Buendia B (2001) Nuclear envelope disorganization in fibroblasts from lipodystrophic patients with heterozygous R482Q/W mutations in the lamin A/C gene. J Cell Sci 114:4459–4468

Wallace AC, Laskowski RA, Thornton JM (1995) LIGPLOT: a program to generate schematic diagrams of protein–ligand interactions. Protein Eng 8:127–134

Wolff N, Gilquin B, Courchay K, Callebaut I, Worman HJ, Zinn-Justin S (2001) Structural analysis of emerin, an inner nuclear membrane protein mutated in X-linked Emery–Dreifuss muscular dystrophy. FEBS Lett 501(2–3):171–176

Yokoyama C, Wang X, Briggs MR, Admon A, Wu J, Hua X, Goldstein JL, Brown MS (1993) SREBP-1, a basic-helix-loop-helix-leucine zipper protein that controls transcription of the low density lipoprotein receptor gene. Cell 75(1):187–197

Young L, Jernigan RL, Covell DG (1994) A role for surface hydrophobicity in protein–protein recognition. Protein Sci 3(5):717–729

Zhang Z, Norris J, Schwartz C, Alexov E (2011) In silico and in vitro investigations of the mutability of disease-causing missense mutation sites in spermine synthase. PLoS One 6(5):e20373